



Parametric modelling of stochastic wave effects on offshore platforms

Yousun Li

Shell Development Company, Houston, TX 77001-0481, USA

&

A. Kareem*

Department of Civil Engineering and Geological Sciences, University of Notre Dame, Notre Dame, IN 46556-0767, USA

(Received 2 July 1991, accepted 26 January 1992)

The time histories of stochastic ocean wave-related processes are simulated by means of computationally efficient parametric models. The parametric models utilized here include the autoregressive and moving averages (ARMA) algorithms for the simulation of wave height fluctuations, discrete convolution models for linear transformations of given time histories, discrete differentiation models for obtaining derivatives, discrete interpolation models for interpolating time series at intermediate time increments and their hybrid combination. The recursive simulation of fluctuation in wave height is accomplished by ARMA algorithm based on a two-stage model-fitting approach that provides simulated processes consistent with the prescribed spectral descriptions. The sensitivity of the model order to the wave spectral description is presented. The parametric simulation schemes of linearly related processes, e.g. wave load effects, are conducted by means of discrete convolution models utilizing finite and infinite wave forms. A parametric model representing differentiation in the context of a linear transformation is employed to simulate derivatives of response processes. A hybrid combination of discrete convolution and differentiation models provides an efficient simulation scheme for evaluating wave loads at the instantaneous position of compliant platforms. Interpolation of time histories is carried out utilizing double subscripted digital filters. The selection of appropriate models and their orders is discussed in the context of their stability, accuracy and robustness. Detailed examples are given to illustrate the practical features of these models.

1 INTRODUCTION

The simulation of random processes has been primarily carried out utilizing methods based on the summation of trigonometric functions (wave superposition) or its modifications such as the use of fast Fourier algorithm (FFT)^{1–4}. The methods based on summation of trigonometric functions are computationally very inefficient. The use of FFT, though, improves the computational efficiency drastically, but not without the expense of increased demand on computer storage. The length of

time series being simulated is often governed by the available computer memory. These shortcomings can be eliminated by employing digital filtering schemes. The parametric time series models in this context, e.g. ARMA, provide recursive relationships that connect the random quantity being simulated at successive time increments.^{5–10} Unlike the FFT-based techniques, this approach does not demand a larger computer memory; rather, only a limited amount of information, e.g. filter coefficient matrices, is stored and long-duration time series may be simulated through recursive relationships. This feature provides the significant computational advantage of digital filtering schemes over FFT-based schemes and the development of these techniques for applications in stochastic mechanics is receiving increasing attention.

*To whom correspondence should be addressed

In this study, parametric models are used to simulate a wide range of random processes related to wave kinematics and wave load effects. Based on the application, these parametric models can be divided into three main categories: the models for simulation of time series from spectral description of one or several correlated stochastic processes (e.g. ARMA models), the models for realization of linear transforms of a given stochastic time series (e.g. discrete convolution and discrete differentiation models), and the models for changing the time increment of simulated time series (e.g. discrete interpolation models). The basic criteria in fitting a parametric model are that the model order should be small and error between the model and target transfer function should not exceed a prescribed limit.

2 BACKGROUND

The ARMA model approach has been used in the ocean, earthquake and wind engineering fields. It has been applied to the simulation of waves. For example, Samii and Vandiver¹¹ developed an ARMA (21,21) model to represent the wave height spectrum which provided very close comparison with the target Bretschneider spectrum. Spanos¹² utilized an ARMA (4,2) to simulate time series for the Pierson–Moskowitz spectrum by allowing some spectral error in the low frequency range. This discrepancy may not be of any significance for general application in offshore dynamics, but for the dynamic analysis of tension leg platforms (TLPs) an accurate modelling in low frequency range may become important. In a subsequent study, Spanos and Mignolet⁸ examined the mathematical peculiarities of the P–M spectrum and presented a Z-transform modelling of P–M wave spectrum. Also, an efficient ARMA model for wave simulation was developed based on an initial AR approximation. This paper addresses issues concerning selection of an ARMA model in the context of stability and accuracy.

The discrete convolution method has been used in the simulation of wave kinematics.¹³ The number of arithmetic operations during the discrete convolution is often large, e.g. Burke and Tighe¹⁴ used 120 multiplications and additions for the simulation of the wave particle velocity at each time interval. Samii and Vandiver¹¹ used a three-step procedure to transform wave kinematics from one location to another utilizing discrete convolutions to account for the vertical and horizontal separations and Hilbert transform for introducing a 90° phase shift. In this study, the time series of wave kinematics and diffraction forces are directly simulated from a reference time history by a discrete convolution filter. This helps to minimize

accumulated errors inherent in the discrete convolution process. The discrete convolution model containing the least number of arithmetic operations introduced here can be established from any given form of the transfer function. The application of the discrete convolution technique in this study is not limited to the wave kinematics and diffraction forces. It is further developed into a discrete retardation form, involving diffraction-radiation considerations, for simulating radiation force based on the platform response.

Discrete differentiation operation is also expressed in terms of a non-recursive model. A hybrid model is introduced which combines features of the discrete convolution and differentiation models.

Interpolation of simulated time series required for changing the time increment is also accomplished by a parametric model with double subscripted coefficients. The model is designed to ensure that it satisfies the stability conditions and meets the prescribed accuracy.

In the following sections a brief discussion of these models, their design considerations and some examples are presented to illustrate the modelling procedures.

3 ARMA MODELS

3.1 AR, MA and ARMA models

Although a discussion of AR, MA and ARMA models is available in numerous papers and texts on signal processing and stochastic processes, a brief introduction is nevertheless included here for the sake of completeness.

An autoregressive (AR) model of order P permits simulation of a stochastic process $y(n\Delta t)$ at time $n\Delta t$ from its previous time histories and corresponding excitation based on the following

$$y(n\Delta t) = - \sum_{r=1}^P A_r y[(n-r)\Delta t] + B_0 \epsilon(n\Delta t) \quad (1)$$

where $\epsilon(n\Delta t)$ is a white noise process with zero mean and unit variance, A_r is the r^{th} AR coefficient, and B_0 denotes a coefficient.

A moving average (MA) model of order Q is a filter that permits simulation of a stochastic process $y(n\Delta t)$ at time $n\Delta t$ based on the previous and present input white noise processes

$$y(n\Delta t) = \sum_{r=0}^Q B_r \epsilon_r[(n-r)\Delta t] \quad (2)$$

in which B_r is the r^{th} MA coefficient.

An autoregressive and moving average (ARMA) model of order P and Q is a filter that permits

simulation of vector $y(n\Delta t)$ at time $n\Delta t$ by its previous time histories and the previous and present white noise processes:

$$y(n\Delta t) + \sum_{r=1}^P A_r y[(n-r)\Delta t] = \sum_{r=0}^Q B_r \epsilon_r[(n-r)\Delta t]. \quad (3)$$

In other words the vector y is defined as an ARMA process of order P and Q if it results from the response of a linear recursive relationship given in eqn (3) to a zero mean and uncorrelated white noise process. It is desirable that the ARMA model orders P and Q are low and the simulated vector $y(\Delta t)$ has an error within prescribed limits. The error in an ARMA model can be expressed in terms of the target and estimated cross-spectral density functions as given below

$$E = \frac{\int_0^{f_{\max}} |\hat{G}(f) - G(f)| df}{\int_0^{f_{\max}} |\hat{G}(f)| df} \quad (4)$$

where E is the error of the estimated spectral density function. The spectral density function estimated from the model is expressed as

$$\begin{aligned} \hat{G}(f) &= 2\Delta t \hat{Y}(f) \hat{Y}^*(f) \\ \hat{Y}(f) &= \left[I + \sum_{r=1}^P A_r \exp(-2\pi f r \Delta t) \right]^{-1} \\ &\quad \times \left[\sum_{r=0}^Q B_r \exp(-2\pi f r \Delta t) \right] \end{aligned} \quad (5)$$

where $\hat{Y}(f)$ represents the Fourier transform of eqn (3), and the superscript * denotes the conjugate operation. Besides the accuracy requirement, an ARMA model must satisfy the stationarity requirement. The necessary and sufficient condition for stationarity of an ARMA model is that all the moduli of the eigenvalues of the matrix Φ should be larger than 1.

$$1 + \sum_{r=1}^P A_r \Phi^r = 0 \quad (6)$$

where Φ^r is a matrix (M, M) defined as the complex roots of the preceding equation. The *maximum entropy method (MEM)*¹⁵ is often utilized to match an ARMA model satisfying the above accuracy and stationarity conditions. In the following sections various methods of fitting an ARMA model to a given spectrum including the maximum entropy method and its approximate forms are discussed.

3.2 AR model and the Yule–Walker equation

In order to simplify the discussion, the ARMA model is

reduced to a unit variate AR model in eqn (1). By post-multiplying eqn (1) with $y[(n-m)\Delta t]$ (in which $0 \leq m \leq n$) and taking expectations

$$\sum_{r=1}^P A_r C_{yy}[(r-m)\Delta t] = -C_{yy}[m\Delta t] \quad (m \neq 0)$$

and

$$B_0^2 = C_{yy}(0) + \sum_{r=1}^P A_r C_{yy}(r\Delta t) \quad (7)$$

where $C_{yy}(r\Delta t)$ denotes the covariance of time series $y(r\Delta t)$. The preceding equations are known as the *Yule–Walker Equations*, and are based on the fact that

$$\begin{aligned} C_{y\epsilon}(m\Delta t) &= 0 \quad \text{for } m > 0 \\ C_{y\epsilon}(m\Delta t) &= B_0 \quad \text{for } m = 0 \end{aligned} \quad (8)$$

and

$$C_{yy}(m) = C_{yy}(-m) = E(y(n\Delta t)y[(n+m)\Delta t]) \quad (9)$$

where $C_{y\epsilon}(m\Delta t)$ denotes the covariance between $y(n\Delta t)$ and $\epsilon(n\Delta t)$.

The Yule–Walker equations can also be written in a matrix form as

$$CA = C' \quad (10)$$

where the Toeplitz matrix, C , contains (P, P) sub-matrices.

$$C = \begin{bmatrix} C_{yy}(0) & C_{yy}(\Delta t) & C_{yy}(P\Delta t) \\ C_{yy}^T(\Delta t) & C_{yy}(0) & C_{yy}[(P-1)\Delta t] \\ C_{yy}[(P-1)\Delta t] & C_{yy}[(P-2)\Delta t] & C_{yy}(0) \end{bmatrix} \quad (11)$$

and A and C' are AR coefficient and covariance matrices: $A = [A_1 A_2 \dots A_P]^T$ and $C' = -[C_{yy}(\Delta t), \dots, -C_{yy}(P\Delta t)]^T$, respectively. The solution of eqn (10) is dependent on the order P of the AR model.

B_0^2 is a positive definite matrix, therefore, following eqns (6) and (7), the Toeplitz matrix (in the right-hand side of eqn (11)) becomes a positive definite matrix. In practice, it is possible that some of the target spectra may not satisfy this condition due to mathematical considerations and numerical round-off errors. Fortunately, experience has shown that wave spectra do satisfy this condition provided some restrictions are imposed. A detailed description of these restrictions will be addressed in the following sections. It can be shown that the Yule–Walker equations also satisfy the *MEM* conditions. In other words, an AR model is an *MEM* model.¹⁶

Despite the convenience of an AR model, one may observe many small peaks in the spectral density function represented by the AR model due to all-pole characteristics of the filter. For example, the zeros of the AR weights of the P–M wave height spectrum are all

within or close to the circle $|z| = 1$ in the complex plane. The estimated spectrum is, therefore, not smooth regardless of the order of AR model.⁸

3.3 ARMA model and the modified Yule–Walker equations

The maximum entropy method may not be computationally convenient to determine the coefficient matrices of an ARMA model because it requires the solutions of a large number of non-linear equations. Alternatively, one of the frequently used methods utilizes the *modified Yule–Walker* equations^{17,18}. This technique is considered to be close to the maximum entropy condition. This method offers a wide range of applications. However, the matching of ARMA coefficients by this method involves the solution of a number of quadratic equations. Also, the simulation of narrow-banded processes such as wave height fluctuations, renders the application of this approach computationally inconvenient due to the numerical singularity of the Toeplitz matrix.

3.4 Two-stage matching for ARMA models

In summary, the AR model characterized by maximum entropy and all-poles is formulated by the solution of a set of linear equations, whereas the ARMA model characterized by poles and zeros is fitted by the solution of a set of non-linear equations. The advantages of both methods are combined by the *two-stage matching method*, in which the ARMA model is obtained from an AR model.

The two-stage matching method can be realized by a few possible schemes.^{7,19} Here the method of the *Auto/Cross-Correlation matching* (ACM) is briefly introduced. This method was utilized by Samarasinghe *et al.*⁷ for fitting a multi-variate ARMA model with the same AR and MA orders. In this study, this method is further extended to include ARMA models with different AR and MA orders.

Let a pre-AR model of order P' be formulated by eqn (7). The ARMA model is based on matching the correlation matrices $C_{yy}(m_p\Delta t)$ with $0 < m_p \leq P$ directly from the target spectra, and cross-correlation matrices $C_{yc}(m_q\Delta t)$ with $0 < m_q \leq Q$ from the pre-AR model according to eqn (8). If both sides of eqn (3) are post-multiplied by $\epsilon[(n - m_q)\Delta t]$ and $y[n - m_p]\Delta t$ in which $m_q = 1, 2, \dots, Q$ and $m_p = 1, 2, \dots, P$ respectively, the following relations are obtained

$$C_{yc}(-m_q\Delta t) + \sum_{r=1}^{\min(m_q, P)} A_r C_{yr}[(r - m_q)\Delta t] = B_{m_q} \quad (12)$$

and

$$C_{yy}(-m_p\Delta t) + \sum_{r=1}^P A_r C_{yr}[(r - m_p)\Delta t] = \sum_{r=0}^Q B_r C_{yr}[(m_p - r)\Delta t]. \quad (13)$$

These two equations may be expressed in a matrix form,

$$\underline{DA} = \underline{C} \quad (14)$$

In the preceding matrix equation, \underline{D} is an $M(P + Q)M(P + Q)$ matrix and consists of four parts

$$\underline{D} = \begin{bmatrix} I & C'^T \\ C' & C \end{bmatrix} \quad (15)$$

where C is the Toeplitz matrix described in eqn (11) and C' contains (PQ) sub-matrices, and the $(r, s)^{th}$ sub-matrix is

$$C'_{rs} = -C_{yr}[(r - s)\Delta t] \quad \text{if } (r \leq s) \quad \text{or} \\ C'_{rs} = 0 \quad \text{otherwise} \quad (16)$$

The matrix A contains coefficient matrices of the ARMA model:

$$\underline{A} = [B_1, B_2, \dots, B_Q, A_1, A_2, \dots, A_p]^T \quad (17)$$

and the matrix C contains $P + Q$ covariance matrices obtained from the pre-AR model and the target cross-spectral density matrix, and it is given by

$$C = [C_{1r}((-\Delta t), \dots, C_{yr}(-Q\Delta t), -C_{1r}(\Delta t), \dots, \\ -C_{yr}(P\Delta t))]^T \quad (18)$$

Based on the experience gained during the course of this study, it is suggested that this approach provides a computationally convenient means of matching the target spectral characteristics for the simulation of wave height fluctuation. Therefore, this method is employed for the study presented here.

4 ARMA MODELS FOR WAVE FIELDS

The P–M and the JONSWAP spectra are used to simulate random wave surface profile at a point.²⁰ The ACM technique is utilized to develop ARMA models for wave surface fluctuation. Typical results are provided in Figs 1 and 2 for the P–M and JONSWAP spectra, respectively. These figures provide the target spectra and estimated spectra from the models. Also included in the figures are the AR and ARMA orders, and the simulation time increment Δt . It is noted that the target and the estimated spectra based on the ARMA models are almost coincident. The order of these models is low and varies between 6 and 20. In the following sections issues concerning guidelines for the order selection

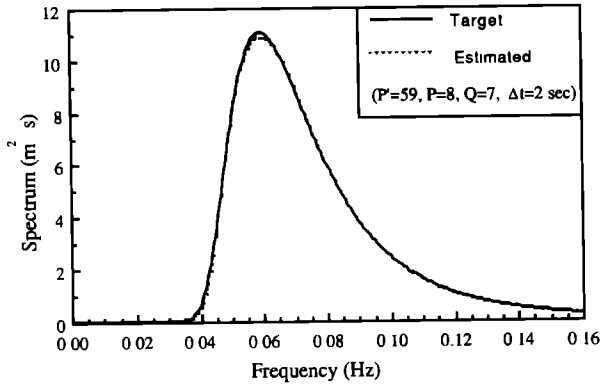


Fig. 1. Comparison of estimated and target spectra (P-M wave surface elevation spectrum).

of the models, in the light of several parameters that influence this selection process, are addressed.

A necessary condition for the existence of a finite AR representation of the process $y(n\Delta t)$ is given by the following²¹

$$\int_0^{f_N} \log[G_y(f)]df > -\infty \quad (19)$$

in which f_N is the Nyquist frequency and $G_y(f)$ is the spectral density function of the process being simulated. The P-M and JONSWAP spectra have a zero of infinite order at the zero frequency that results in violating the preceding inequality. Regarding the P-M spectra, Spanos¹² modified the spectral description such that the order of zero at the zero frequency was changed from infinity to 27 by introducing a Taylor series expansion, thus satisfying the above inequality. It is noted during the course of this study that the preceding inequality (eqn (19)) is violated for nearly all forms of wave spectra due to numerical round-off error and underflow problems within a certain low frequency range.^{22,10} In order to overcome this difficulty, in this study white noise with a very small variance was added in the target spectra. In the examples shown in Figs 1 and 2, white noise of spectral ordinate ranging $(0.0001 \sim 0.001)\sigma^2/f_N$ was added to the target spectrum, where σ^2 represents the overall variance associated with the spectra²¹. It is important that the added noise should be small enough that its influence

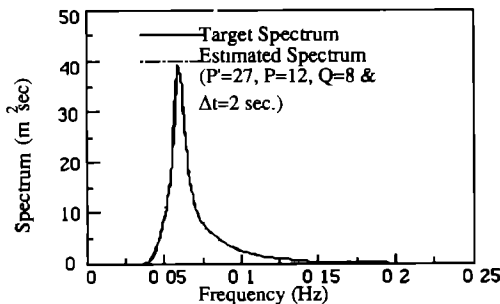


Fig. 2. Comparison of estimated and target spectra (JONSWAP waves spectrum).

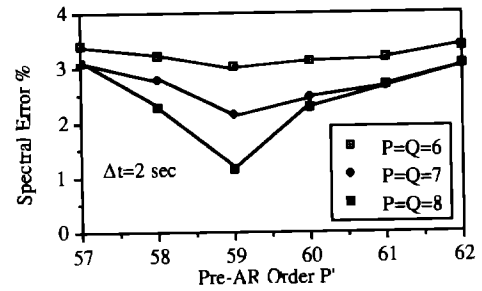


Fig. 3. Spectral error versus pre-AR order P' (P-M wave spectrum)

does not introduce any sizeable addition to the wave surface profile. The introduction of white noise offers robustness and precludes any other pre-modelling mathematical manipulation necessary otherwise

The next step involves the selection of pre-AR order, P' , and the orders P and Q for the ARMA model. In order to reduce the number of parameters in this two-step selection process, one may impose the condition $P = Q$. Subsequently, for a fixed P' , different choices of $P = Q$ can result in different levels of errors as noted in Figs 3 and 4 for the P-M and JONSWAP ($\gamma = 3.3$) spectra. The spectral error is defined as the integral of the difference between estimated and target spectra normalized by the integral of the target spectra up to the Nyquist frequency. It is noted that the higher pre-AR order does not necessarily result in an ARMA model with a lower spectral error. For wide-banded processes such as wind fluctuation, it is found that an increase in pre-AR order generally provides a favorable decrease in the spectral error.²³ However, for the narrow-banded wave height fluctuation the spectral error is minimum at a certain value and as such does not follow any distinct trend

Although ARMA models with equal AR and MA orders are widely reported in the literature, in the present study it is found that different AR and MA orders may improve the model accuracy, especially for the narrow-banded process. For the P-M spectrum, $P = 8$ and $Q = 7$ provides lower spectral error in comparison with the model based on $P = Q = 7$ with P' being equal to 59 in both cases (Fig 5). The JONSWAP wave elevation spectrum for $P' = 27$ and

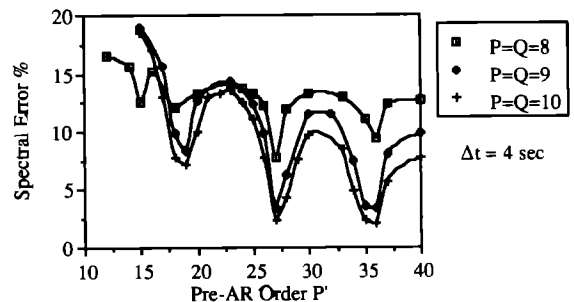


Fig. 4. Spectral error versus pre-AR order (JONSWAP wave spectrum)

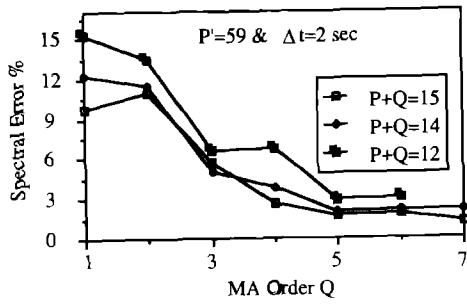


Fig. 5. Spectral error versus MA order (P-M wave spectrum)

$P + Q = 16$, in which $P = 12$ and $Q = 4$, provides generally lower error as compared to the case where $P = Q = 8$ (Fig. 6).

It is noted that for the cases in which Q is greater than P , not only results in a lower accuracy but also leads to a non-positive definite matrix in eqn (16). This results in a non-stationary ARMA model. Therefore, it is recommended that $P \geq Q$ to alleviate these problems.

In summary, P' , P and Q are three independent parameters, and only by a suitable combination of these parameters, one can obtain the optimal ARMA model. The choice of these parameters is generally made rather empirically utilizing an interactive computer code.¹⁰ Samaras *et al*⁷ have suggested the following guidelines

$$P' > P + Q + 2 \quad (20)$$

However, it is found in Fig. 4 that for the JONSWAP spectrum a model with $P' = 19$ and $P = Q = 10$ provides an optimal choice for $P' < 25$, but it does not meet the above guideline

5 DISCRETE CONVOLUTION MODELS

The wave-related processes are fully coherent. Therefore, a set of fully-coherent random processes may be simulated by a convolution with a reference random process utilizing an appropriate kernel. The wave surface profile, wave kinematics and the associated wave-induced forces which are all fully

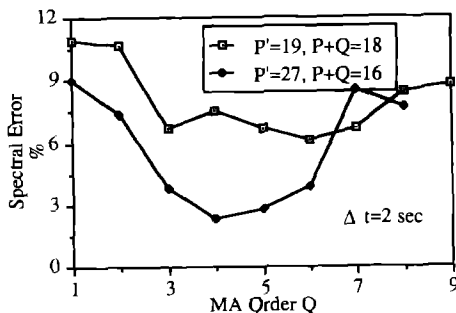


Fig. 6. Spectral error versus MA order (JONSWAP wave spectrum)

coherent processes are simulated in this study by a convolution of a reference process, i.e. wave elevation, $\eta(t)$, at the origin of the space-fixed coordinate system, with the corresponding kernels^{11,13,24} However, the preceding convolution involves an integral over an infinite time period which may impose computational difficulties. In order to overcome this difficulty attention is focused here on simplifying techniques in which these integrals are recast in nonrecursive digital models involving a limited number of arithmetic operations.

Let the transfer function between a random process $Y(t)$ and the reference process $\eta(t)$ be given by the following

$$H(f) = \frac{Y(f)}{\eta(f)} \quad (21)$$

where $Y(f)$ and $\eta(f)$ = Fourier transform of $y(t)$ and $\eta(t)$, respectively. The convolution kernel $h(t)$ corresponding to the transfer function, $H(f)$, is given by

$$h(t) = \int_{-\infty}^{+\infty} H(f) \exp(j2\pi ft) df. \quad (22)$$

The random process $y(t)$ can be simulated for known $\eta(t)$ by the convolution given below

$$y(t) = \int_{-\infty}^{+\infty} h(\tau) \eta(t - \tau) d\tau \quad (23)$$

The integration over a time period $-\infty$ to $+\infty$ in the preceding equation needs to be evaluated numerically. If the preceding integral is performed by the trapezoidal rule, and the infinite time may be truncated into a finite length of time from T_- to T_+ , then the discrete form of the preceding equation may be recast in the following form

$$y(n\Delta t) = \sum_{r=-Q^-}^{Q^+} h_r \eta[(n-r)\Delta t] \quad (24)$$

where the discrete convolution coefficients h_r are equal to $h(r\Delta t)\Delta t$, in which $r = -Q^-, \dots, -2, -1, 0, 1, 2, \dots, Q^+$ and the discrete convolution orders Q^- and Q^+ are given by

$$Q^- = \frac{T_-}{\Delta t} \quad \text{and} \quad Q^+ = \frac{T_+}{\Delta t} \quad (25)$$

It is desirable to keep the order of the preceding discrete convolution model to a minimum and at the same time to minimize the error introduced by discretizing the convolution integral. The discrete convolution model can be formulated from the discrete Fourier transformation of finite and infinite duration waveforms.²⁵ Both approaches have their merits and applications

5.1 Discrete convolution model utilizing the finite duration waveforms

Let the frequency range from zero to Nyquist frequency be discretized at Q discrete frequencies. The discrete inverse Fourier transform of $H(f)$ is given by

$$\hat{h}(r\Delta t) = \left\{ \sum_{s=1}^{Q-1} H^*(s\Delta f) \exp\left(-j\pi \frac{rs}{Q}\right) + \sum_{s=0}^Q H(s\Delta f) \exp\left(j\pi \frac{rs}{Q}\right) \right\} \Delta f \quad (26)$$

for $r = -Q + 1, \dots, -1, 0, 1, \dots, Q$ and $\Delta f = 1/2Q\Delta t$. The corresponding coefficients of the discrete convolution are given by

$$h_r = \hat{h}(r\Delta t)\Delta t \quad (27)$$

which has the order $Q^+ = Q$ and $Q^- = Q - 1$ (total order is $2Q$, including zeroth coefficient).

If the transfer function is a real variable (e.g. the second-order derivative), the model of order Q in eqn (24) appears as given below

$$y(n\Delta t) = \sum_{r=1}^{Q-1} h_r \{ \eta[(n-r)\Delta f] + n(n+r)\Delta f \} + h_0 \eta(n\Delta f) + h_Q \eta[(n-Q)\Delta f] \quad (28)$$

in which the coefficients $h_r (r = 0, 1, \dots, Q)$ are given by

$$h_r = \left\{ H(0) + H(Q\Delta f) + 2 \sum_{s=1}^{Q-1} H(s\Delta f) \times \cos\left(j\pi \frac{rs}{Q}\right) \right\} \Delta f \Delta t \quad (29)$$

and the corresponding estimated transfer function is

$$\hat{H}(s\delta f) = \sum_{r=1}^{Q-1} 2h_r \cos\left(2\pi \frac{rs}{L}\right) + h_0 + h_Q \quad (30)$$

where L is the total length of the time series. Similarly, for the imaginary transfer functions (e.g. derivative), the recursive model of order $Q - 1$ is given by

$$y(n\Delta t) = \sum_{r=1}^{Q-1} h_r \{ \eta[n-r]\Delta t - \eta[n+r]\Delta t \} \quad (31)$$

where the coefficients $h_r (r = 1, 2, \dots, Q - 1, \text{ total } Q - 1 \text{ terms})$ are given below

$$h_r = \sum_{s=1}^{Q-1} 2H(s\Delta f) \sin\left(\pi \frac{rs}{Q}\right) \Delta t \Delta f \quad (32)$$

and the corresponding estimated transfer function is given by

$$\hat{H}(s\delta f) = \sum_{r=1}^{Q-1} 2h_r \sin\left(2\pi \frac{rs}{L}\right). \quad (33)$$

In a general case, taking discrete Fourier transformation of both sides of eqn (24) leads to the estimated transfer function,

$$\hat{H}(s\delta f) = \frac{Y(s\delta f)}{\eta(s\delta f)} = \sum_{r=1-Q}^Q h_r \exp\left(-j2\pi \frac{rs}{L}\right) \quad (34)$$

The frequency increment δf in the discrete Fourier transform of $Y(s\delta t)$ is

$$\delta f = \frac{1}{L\Delta t} \quad (35)$$

The length L of a discrete process to be simulated is an arbitrary integer number, and generally $Q \ll L$. It is a *discrete convolution of an infinite and a finite duration waveform* (see Ref. 25). Let $2L = \beta Q$ in which β is a positive integer number. In this case at the frequency equal to $\beta n \delta f$ (where n is an integer) the transfer function estimated from the model is just the inverse discrete Fourier transform of eqn (26). Thus, the model transfer function is exactly the target transfer function expressed by eqn (21).

$$\hat{H}(\beta n \delta f) = H(\beta n \delta f). \quad (36)$$

However, at frequency $(\beta n + \alpha)\delta f$ with $\alpha < \beta$, $\hat{H}[(\beta n + \alpha)\delta f]$ generally provides a poor representation of the transfer function between $H(\beta n \delta f)$ and $H[(\beta n + 1)\delta f]$. Many tests in this study showed that this approach is mainly useful for some real transfer functions. For example, it may be used to fit the fourth-order derivative for real transfer functions. It is demonstrated in Fig. 7 that the total model order $Q = 5$ yields six points coincident with the exact transfer function. With an increase in the model order to $Q = 23$, the number of coincident points increases to 24. Accordingly, there is a significant improvement in the high frequency part as is shown in Fig. 8. However, in the low frequency part as seen in Fig. 9 (which zooms in on the low frequency part) the estimated transfer function with $Q = 23$ exhibits oscillations. If this method is used in odd-order derivatives, e.g. the third-order derivative for the imaginary transfer function (Fig. 10), there is an error in the high frequency part in addition to the error in the low frequency part that is the

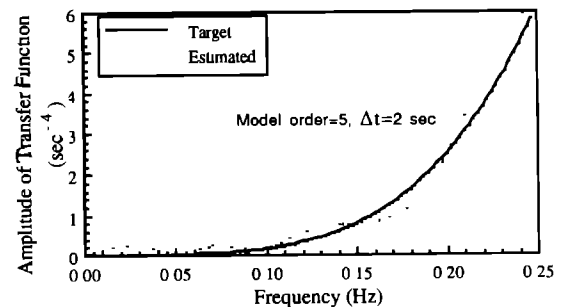


Fig. 7. Comparison of estimated and target transfer functions (fourth-order derivative)

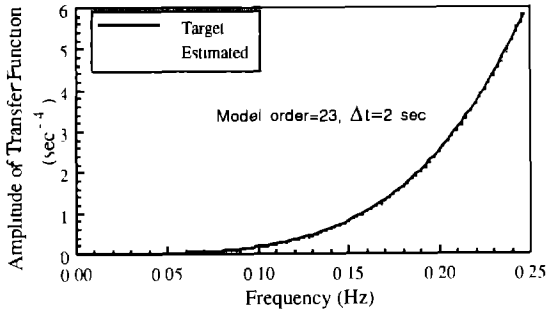


Fig. 8. Comparison of estimated and target transfer functions (fourth-order derivative)

same as the even order derivative. The error reduces slowly with an increase in the model order.

5.2 Discrete convolution models utilizing infinite duration waveform

An alternative method is to let the number of frequencies Q in eqn (26) be much larger than any possible length of the time series. As a result eqn (26) becomes a *discrete convolution of two infinite duration waveforms*. In the order to make this practical, let the discrete convolution model order in eqn (24) (here it denotes by N_f) approach infinity and truncate it at orders Q^+ and Q^- . This is only possible provided the following two convergence conditions are satisfied:

$$\lim_{N_f \rightarrow \pm\infty} \hat{h}(r\Delta t) = h(r\Delta t) \quad (37)$$

where $\hat{h}(r\Delta t)$ is the discrete Fourier transform of transfer function $H(r\Delta f)$, and $h(r\Delta t)$ is an exact transfer function, and

$$\lim_{r \rightarrow \pm\infty} h(r\Delta t) = 0 \quad (38)$$

These convergence requirements also imply the following

- (1) The discrete Fourier transform of $H(r\Delta f)$ with $r = 1, 2, \dots, N_f$ is close to the discrete Fourier transform of $H(r\Delta f)$ with $r = 1, \dots, N_f + 1$
- (2) $\hat{h}(r\Delta t) < e h_{\max}$ for all $r > Q^+$ and $r < -Q^-$, in which Q^+ and Q^- are positive integers, e is the coefficient convergence indicator, e.g. 2%, and

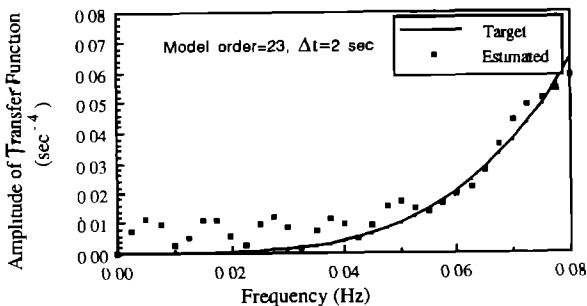


Fig. 9. Comparison of estimated and target transfer functions (fourth-order derivative)

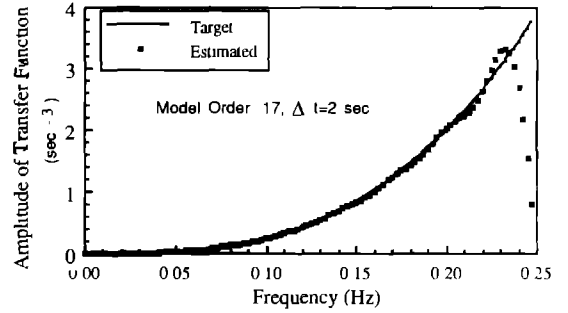


Fig. 10. Comparison of estimated and target transfer functions (third-order derivative).

h_{\max} is the maximum value of all the estimated convolution kernels. Furthermore, the model order should be large enough to account for the low frequency part. A number of test runs in this study suggest that $2/(Q^+ + Q^-)\Delta t \leq f_{\min}$, where f_{\min} is the minimum frequency of interest.

Considering the fact that in practice only the positive frequencies in the discrete Fourier transforms are used, the coefficients of the discrete convolution model representing convolutions of two infinite duration waveforms are given by

$$h_r = \hat{h}(r\Delta t) \quad \text{for } 0 \leq r \leq Q^+$$

$$h_r = \hat{h}[(2N_f + 1 + r)\Delta t] \quad \text{for } -Q^- \leq r < 0 \quad (39)$$

where the discrete inverse Fourier transform in eqn (26) is given by

$$\hat{h}(r\Delta t) = \lim_{N_f \rightarrow \infty} \sum_{s=0}^{2N_f-1} H(s\Delta f) \exp\left(j\pi \frac{rs}{N_f}\right) \quad (40)$$

and the transfer function $H(s\Delta f)$ with $s > N_f$ is a reflection of $H(s\Delta f)$ with $s < N_f$

$$H[(2N_f + 1 - s)\Delta f] = H^*(s\Delta f). \quad (41)$$

The corresponding discrete convolution model is given by

$$y(n\Delta t) = \sum_{r=-Q^-}^{Q^+} h_r \eta[(n-r)\Delta t] \quad (42)$$

The estimated transfer function by the discrete convolution model is expressed by the following

$$\hat{H}(f) = \sum_{r=-Q^-}^{Q^+} h_r \exp(-j2\pi fr\Delta t) \quad (43)$$

A discrete convolution model has a *valid frequency range* within which the estimated transfer function is close to the target one. The *valid maximum frequency* f_{\max} is the Nyquist frequency $1/(2\Delta t)$ and the *valid minimum frequency* f_{\min} depends on the total model order $Q^+ + Q^- + 1$. It is recommended to use the relation $2/(Q^+ + Q^-)\Delta t \geq f_{\min}$

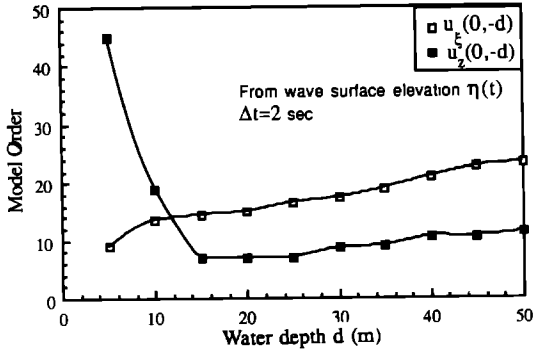


Fig. 11. Discrete convolution model order for describing wave particle velocities.

The preceding convergence criteria may be satisfied by both real and complex transfer functions. Test cases have shown that the wave-related processes, such as the wave surface elevation, wave particle velocity and global wave diffraction force on a rigid body, such as TLP can satisfy the convergence requirement. A mathematical description of the conditions of convergence for a transfer function in a general form is beyond the scope of this presentation. Only a few examples of the several cases examined in this study will be given in the following sections.

5.3 Discrete convolution models for the wave-related processes

Let us define the wave surface elevation at (0,0,0) in the space-fixed coordinate system as the reference time series which is generated by an ARMA model described in the previous section. The transfer functions that relate the wave surface elevation to the horizontal and vertical wave particle velocities are given by

$$H_{u_{\xi}-\eta}(f) = 2\pi f \exp(kz) \exp(-jk\xi)$$

and

$$H_{u_z-\eta}(f) = j2\pi f \exp(kz) \exp(-jk\xi) \quad (44)$$

where $H_{u_{\xi}-\eta}(f)$ and $H_{u_z-\eta}$ represent transfer functions that relate wave surface elevation to horizontal and vertical water particle velocities, k is the wave number, ξ

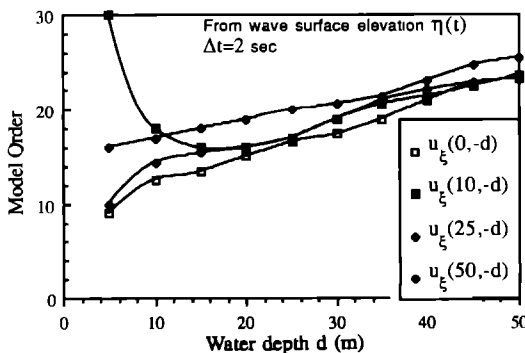


Fig. 12. Discrete convolution model order for wave particle velocities at different locations in the horizontal direction.

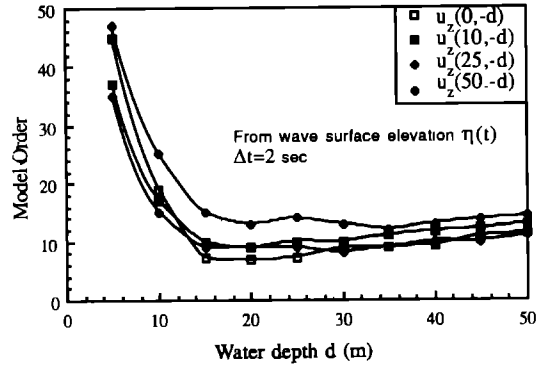


Fig. 13. Discrete convolution model order for vertical component of wave particle velocities

is the horizontal location along the direction of wave propagation and z is the vertical location

The basic objective in the selection of a parametric model is to have the lowest order filter with an acceptable level of error. There are a number of factors which influence the filter order. Figures 11–13 illustrate how the order of the discrete convolution model describing the horizontal and vertical wave particle velocities is influenced by the vertical location of a point. Generally, near the water surface for the vertical component of water particle velocity, a higher order model is required. In these figures $u_{\xi}(10,-d)$ and $u_z(10,-d)$ etc. denote the horizontal and vertical velocities at $\xi = 10$ and $z = -d$. The results in Fig. 14 show that the time increment Δt has a significant influence on the model order. A larger value of time increment tends to reduce the significant influence on the model order. A larger value of time increment tends to reduce the model order.

A suitable choice of the reference time series is also very important. Figure 15 demonstrates the reason for choosing water surface elevation as the reference time series instead of the horizontal water particle velocity, which could require a discrete convolution model of order as high as 180

The fact that the model orders are high for wave particle velocities at locations close to water surface implies that a better reference time series representing an

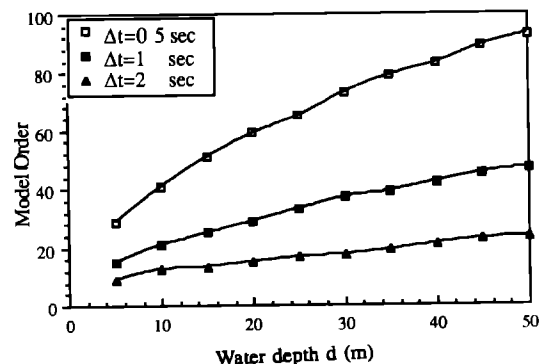


Fig. 14. Discrete convolution model order for wave particle velocities at different depths and time increments.

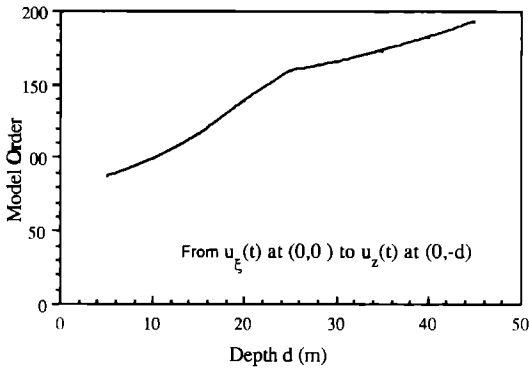


Fig. 15. Discrete convolution model order for relating different components of wave particle velocities

arbitrary wave surface elevation can be used to reduce the model order, which is defined by

$$\eta^l(f, z^l) = \exp(kz^l)\eta(f) \quad \text{with } z^l > 0 \quad (45)$$

This modification has little physical meaning, but serves as a means of shifting Figs 12–13 to the right by a distance z^l . The corresponding transfer functions for the horizontal and vertical wave particle velocities are given by

$$H_{u_{\xi}-\eta}I(f) = 2\pi f \exp[k(z + z^l)] \exp(-jk\xi)$$

and

$$H_{u_z-\eta}I(f) = j2\pi f \exp[k(z + z^l)] \exp(-jk\xi) \quad (46)$$

The discrete convolution model can also be used to simulate wave elevations at a desired horizontal location ξ , which causes viscous drift forces in the splash zone of the structure. The transfer function of $\eta(\xi, t)$ with respect to $\eta(t)$, is

$$H_{\eta(\xi)-\eta}(f) = \exp(-jk\xi) \quad (47)$$

Similarly, the diffraction force vector $F_s(t)$ acting on a rigid body of large size in terms of wavelength is simulated by the discrete convolution models. The convolution filter coefficients are obtained by the inverse Fourier transform of the transfer function vector $H_{F_s-\eta}(f)$. The diffraction

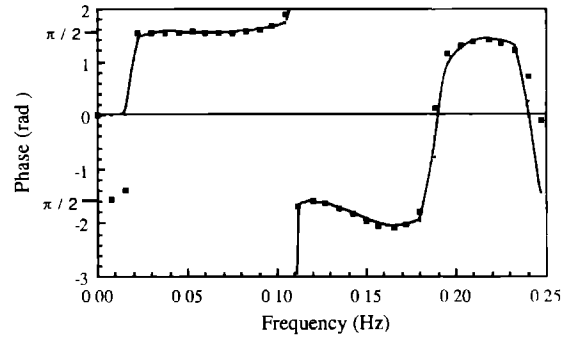


Fig. 17. Diffraction phase (surge)

transfer function vector $H_{F_s-\eta}(f)$ may be obtained by the boundary element method, which accounts for the diffraction force on a rigid body by a deterministic wave of frequency f and unit elevation. Figures 16–21 illustrate comparison of the amplitudes and phases of the target transfer functions with those estimated from the discrete models for a typical TLP. An excellent agreement is noted in these figures. These digital filters provide a very useful input to a time domain analysis of a TLP exposed to random waves.

The preceding approach for simulating time series of wave kinematics and diffraction forces utilizing convolution techniques is different from the methods reported in the literature. For example, Sami and Vandiver¹¹ simulated the wave particle velocities at any location by three convolutions representing the vertical attenuation, horizontal wave propagation and Hilbert transform (90° phase change). Each discrete convolution has a specified form. A succession of convolutions may result in accumulation of error. However, by utilizing the method developed in this study, it is possible to obtain the discrete convolution model according to any transfer function. The wave kinematics at any location can be simulated by one discrete convolution model. Thus, both the accumulated error and the total number of arithmetic operations may be reduced. Furthermore, it becomes possible to simulate the time series of the wave diffraction forces by the transfer functions obtained from the boundary element method.

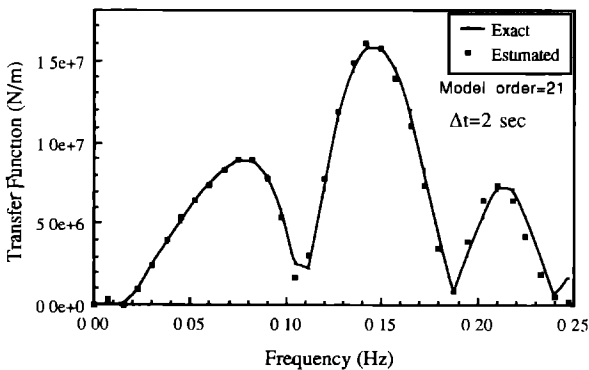


Fig. 16. Diffraction transfer function (surge).

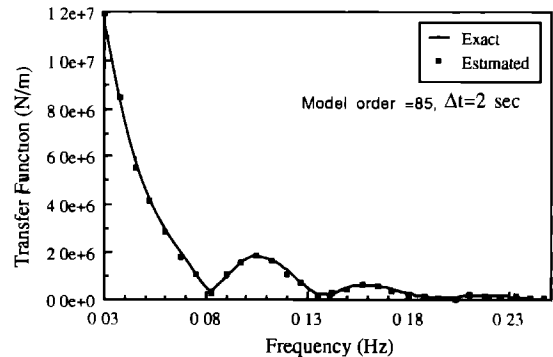


Fig. 18. Diffraction transfer function (heave)

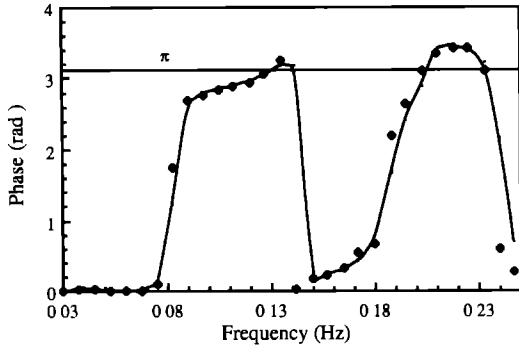


Fig. 19. Diffraction phase (heave)

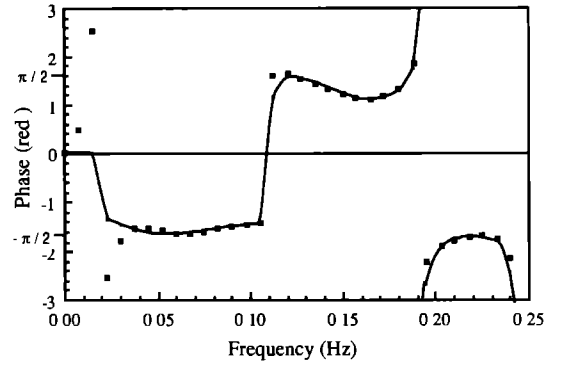


Fig. 21. Diffraction phase (pitch)

5.4 Special form of discrete convolution model

The coefficients of a convolution model in some cases may have an analytical form whose characteristics can be utilized to form a nonrecursive model with a low order and high accuracy. The case in point is for example a quadrature filter. Its transfer function is all-pass with a 90° phase shift (e.g. from vertical to horizontal wave particle velocity)

$$H(f) = -j \operatorname{sgn}(f) \quad (48)$$

The response of a quadrature filter to a process with real values only is called the *Hilbert transform* (see Ref 26). The Hilbert transform has been utilized for the simulation of the vertical wave particle velocity $u_z(t, r)$ from the horizontal wave particle velocity $u_\xi(t, r)$ at the location r .¹¹ The analytical form of the convolution is given by²⁶

$$u_z(t) = -u_\xi(t) * \frac{1}{\pi t} = \frac{1}{\pi} \int_{-\infty}^{+\infty} \frac{u_\xi(\tau)}{t - \tau} d\tau \quad (49)$$

The elevation of the preceding expression is not numerically efficient. A discrete form of the Hilbert transform was developed in this study. By imposing that the cut-off frequency be equal to the Nyquist frequency, the convolution kernel of the Hilbert transform is expressed by the following:

$$h_r = \left\{ \int_0^{\frac{1}{2\Delta t}} j \exp(j2\pi fr \Delta t) df - \int_0^{\frac{1}{2\Delta t}} j \exp(-j2\pi fr \Delta t) df \right\} \Delta t \quad (50)$$

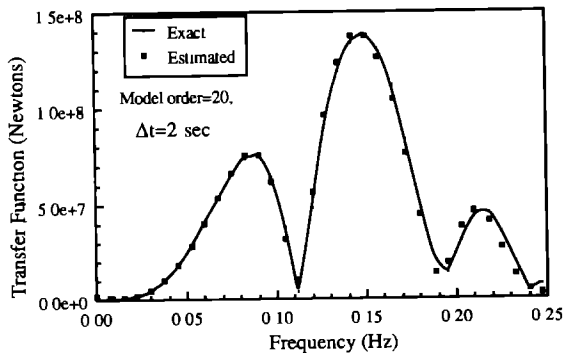


Fig. 20. Diffraction transfer function (pitch).

which, after integration reduces to

$$h_r = \frac{2}{\pi r} \quad \text{for } r = \pm 1, \pm 3, \pm 5, \dots,$$

and

$$h_r = 0 \quad \text{for } r = 0, \pm 2, \pm 4, \dots \quad (51)$$

Another example is the transfer function between two time processes $Y(t)$ and $\eta(t)$ given by

$$H_{Y-\eta}(f) = 2\pi f. \quad (52)$$

The discrete convolution coefficients of this function are

$$h_r = \pi / (2\Delta f) \quad \text{for } r = 0$$

$$h_r = -2 / (\pi r^2 \Delta t) \quad \text{for } r = \pm 1, \pm 3, \pm 5, \dots,$$

and

$$h_r = 0 \quad \text{for } r = \pm 2, \pm 4, \pm 6, \dots \quad (53)$$

The above two examples have the following characteristic features

- (1) Symmetry of the model coefficients, i.e. $h_r = h_{-r}$, reduces the total multiplications to a half.
- (2) The model coefficients h_r are equal to 0 if r is an even number except for $r = 0$. This feature reduces multiplication by another half.
- (3) Convergence in the discrete convolution coefficients is rapid, especially in the second example.
- (4) The convergence of coefficients with $r \rightarrow \infty$ is independent of the time increment Δt .

The corresponding convolution model can be simply recast in the following form:

$$y(n\Delta t) = h_0 \eta(n\Delta t) + \sum_{r=1}^Q h_r \{ \eta[(n - 2r + 1)\Delta t] \pm (n + 2r - 1)\Delta t \} \quad (54)$$

in which ‘-’ represents the first case and ‘+’ the second case. By utilizing these features, the order of a model may be reduced. An application of this approach will be shown in the description of the hybrid model in a later section.

6 DISCRETE RETARDATION MODEL

The simulation of fully coherent random processes with respect to a reference process utilizing discrete convolution models was highlighted in the preceding sections. Typically, the wave particle kinematics are simulated from the fluctuations in the wave surface elevation at a reference location. The simulated process at any time is viewed as a linear combination of the past, the present and the future time histories of the reference process. However, in some cases the future time history of the reference process is unknown, for example, the structural response $X(t)$ which is taken as the reference process for simulating radiation force. It may be possible to express the time process to be simulated as a linear combination of the past and present time history of the reference process only in terms of a *one-sided discrete convolution model*

$$y(n\Delta t) = \sum_{r=0}^Q h_r x[(n-r)\Delta t] \quad (55)$$

where

$$h_r = \lim_{N_f \rightarrow \infty} \sum_{s=0}^{N_f} H(s\delta f) \exp\left(j2\pi \frac{sr}{N_f}\right) \delta f \Delta t \quad (56)$$

However, the convergence requirement of the convolution kernels for $N_f \rightarrow \infty$ in one-sided discrete convolution are only satisfied in some special cases.

In order to circumvent this difficulty, each particular application needs to be examined individually. A typical example is the radiation force, $f_R(t)$, which describes the loads induced by a large rigid body oscillating with displacement amplitude given by vector $x(t)$ in an otherwise still water. The radiation force is generally expressed in the frequency domain. Its Fourier components $F_R(f)$, are related to the Fourier components of the displacement, $X(f)$, by the added mass $A(f)$ and radiation damping $C(f)$

$$F_R(f) = -A(f)X(f) - C(f)X(f)$$

The time history of the radiation force is expressed in terms of the added mass and radiation damping by the following equation²⁷

$$f_R(t) \approx \hat{A}\dot{x}(t) + \int_0^\infty c(\tau)\dot{x}(t-\tau)d\tau \quad (57)$$

where the *retardation function matrix* $c(t)$ is given by

$$c(t) = 4 \int_0^\infty C(f) \cos 2\pi ft df \quad (58)$$

and the constant added mass matrix is

$$\hat{A} \approx A(f_0) + \frac{1}{2\pi f_0} \int_0^\infty c(t) \sin 2\pi f_0 t dt \quad (59)$$

with $f_0 =$ system natural frequency

Accordingly, the radiation force in the discrete form can be simulated by a *discrete retardation model* as defined below

$$f_r(n\Delta t) = -Ax(n\Delta t) - C_0 x(n\Delta t) - \sum_{r=1}^Q C_r \dot{x}[(n-r)\Delta t] \quad (60)$$

where the retardation coefficients are obtained by the discrete cosine transform,

$$C_r = \frac{4}{Q} \sum_{s=1}^Q C(s\Delta f) \cos\left(\frac{2\pi sr}{Q}\right) \quad (61)$$

in which Q is the model order and the retardation added mass is given by

$$\hat{A} \approx A(f_0) + \frac{1}{2\pi f_0} \sum_{r=0}^\infty C_r \sin(2\pi f_0 r \Delta t) \quad (62)$$

The quality of the retardation model may be assessed by comparing the added mass and radiation damping estimated from the retardation model with the exact ones expressed on the left-hand side of eqn (57). The estimated added mass matrix is obtained by taking the Fourier transform of both sides of eqn (60)

$$\hat{A}(f) = A - \frac{1}{2\pi f} \sum_{r=1}^Q C_r \sin(2\pi fr \Delta t) \quad (63)$$

and the estimated radiation damping coefficient is given by

$$\hat{C}(f) = \sum_{r=0}^\infty C_r \cos(2\pi fr \Delta t) \quad (64)$$

Examples concerning a typical TLP are given in Figs 22–25. The model coefficients are obtained from the convolution kernel of finite duration waveform described earlier in this paper. These figures demonstrate that the estimated and exact radiation dampings are in good agreement, whereas there are some discrepancies between the estimated and exact added mass due to imposing frequency independence.

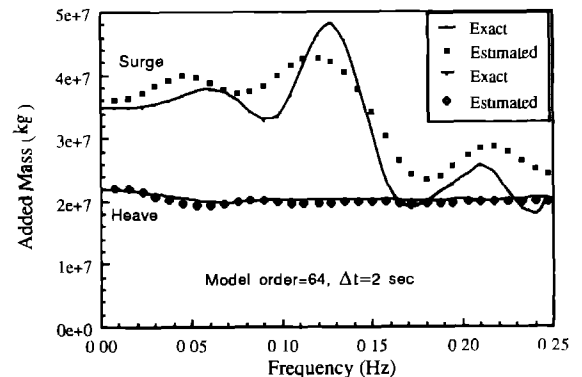


Fig. 22. Added mass using retardation model (surge and heave)

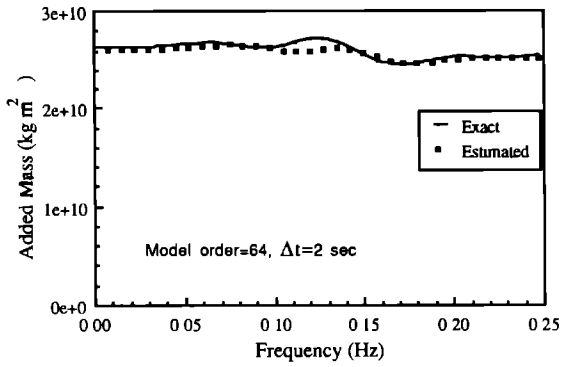


Fig. 23. Added mass using retardation model (pitch).

to the constant added mass. However, a correct representation of radiation damping (Fig. 25) may be more important. The error in the simulation of the platform response caused by the approximation of the added mass (Fig. 22) may not be very significant.

7 DISCRETE INTERPOLATION MODEL

It has been stated earlier that the time histories of the wave height fluctuation may not be simulated at the time increment equal to that required by the numerical scheme involving time integration of the equations of motion. The reason for this different time increment is primarily due to the following: (1) The time increment in a numerical integration scheme for the solution of the dynamic equations of motion needs to be smaller than any natural period of the dynamic system to ensure numerical stability and accuracy. Also the time increment must be smaller than the lowest period at which the input loading contains significant energy. (2) Different load processes, for example, wind, and earthquake processes, have different time increments after they are simulated by their own respective parametric models. Therefore, a *Discrete Interpolation Model* is needed to interpolate a time series with time increment Δt into a time series with desired time increment δt .

A discrete interpolation model must satisfy the following conditions (in this manner a discrete process $y(n\Delta t)$ in which n is an integer, becomes the discrete

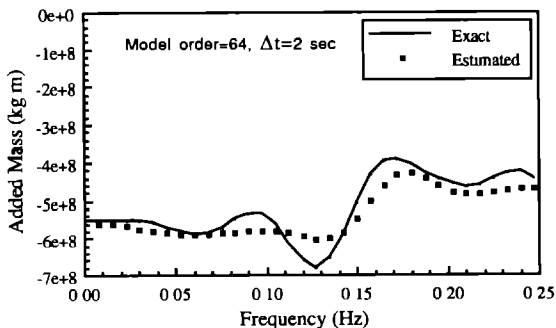


Fig. 24. Added mass using retardation model (surge-pitch)

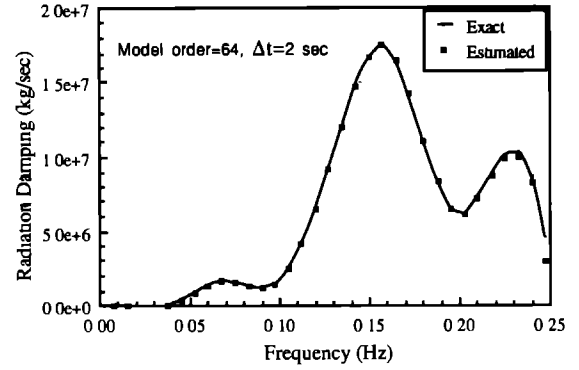


Fig. 25. Radiation damping using retardation model (surge) process $Y[(n + \alpha)\Delta t]$ in which α is a fraction number

- (1) *Local Interpolation*: $y[(n + \alpha)\Delta t]$ is interpolated according to $Y[(n + r)\Delta t]$ with $r = -Q^-, \dots, -2, -1, 0, 1, 2, \dots, Q^+$ in which Q^- and Q^+ are small integers. The conventional global interpolation involving all the input data is not suitable for the present application
- (2) *Accuracy*: The interpolation changes the Nyquist frequency from $1/(2\Delta t)$ to $1/(2\delta t)$. The spectral density function is expected to remain the same for the frequencies lower than $1/(2\Delta t)$ and zero with the frequency range $1/(2\Delta t)$ to $1/(2\delta t)$. The ideal transfer function of an interpolation model is unit for $f < 1/(2\Delta t)$ and 0 for $1/(2\delta t) > f > 1/(2\Delta t)$

The trigonometric interpolation has been frequently used in interpolation of random processes. Li and Kareem²³ further expressed it into a discrete convolution form with double subscripted coefficients

$$y[S(n + \beta)\delta t] = \sum_{r=-Q^+}^{Q^+} h_{\beta r} y[(n + r)\Delta t] \quad (65)$$

in which $2Q^+$ is the interpolation order, $S = \Delta t/\delta t$ is an integer, and $\beta = 0, 1, 2, \dots, S-1$. In reality, this is a convolution of two finite duration waveforms. The double subscripted coefficients are derived from the Fourier transform of transfer function $H(m\Delta f)$,

$$h_{\beta r} = \sum_{m=-SQ^+}^{SQ^+} H(m\Delta f) \times \exp\left(j\pi \frac{mr'}{SQ^+}\right) / (2Q^+) \quad \text{with } r' = rs + \beta \quad (66)$$

in which

$$H(m\Delta f) = 1 \quad \text{for } -Q^+ \leq m \leq Q^+$$

$$H(m\Delta f) = \frac{1}{2} \quad \text{for } m = \pm(Q^+ + 1)$$

$$H(m\Delta f) = 0$$

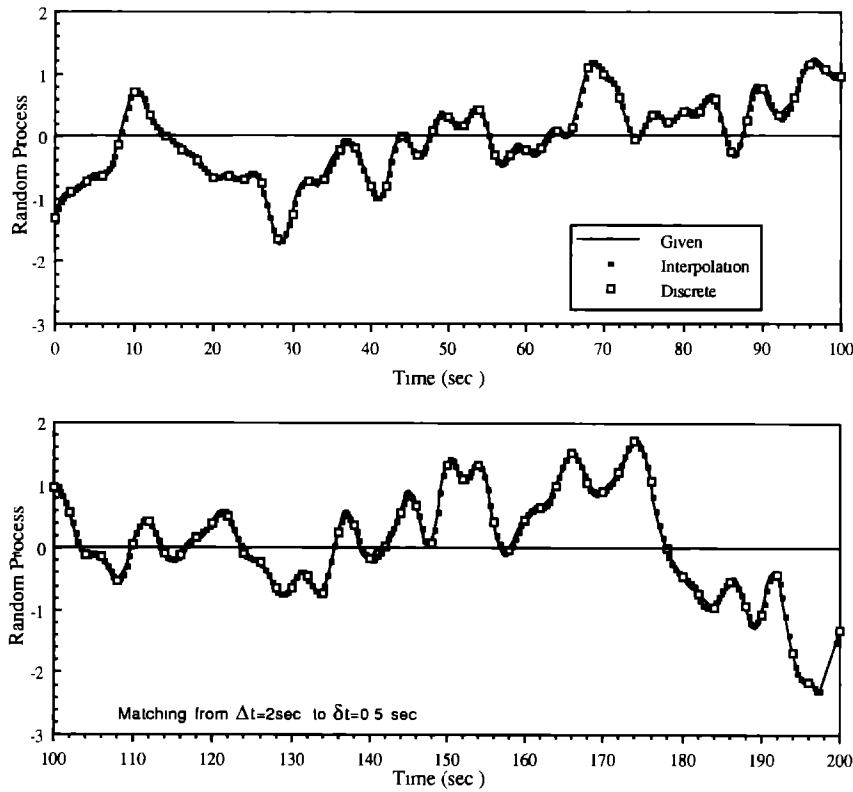


Fig. 26. a. Continuous, discrete and interpolated time series (0–100 seconds) b Continuous, discrete and interpolated time series (100–200 seconds)

for $Q^I + 1 < m \leq SQ^I$ and $-Q^I - 1 > m \geq -SQ^I + 1$ and $\Delta f = 1/2Q\Delta t$

With the increasing value of order $2Q^I$, the accuracy is increased. It is recommended to use $Q^I = 8 \sim 10$. Figure 26 provides an example, in which the solid line is the known continuous random process, the empty squares are discrete time series of time increment Δt picked from the continuous time process, and then black squares are the discrete time series of small time increment δt obtained by interpolating the time series represented by empty squares. A good agreement between the known time process and the discrete time series obtained by interpolation is observed. The main advantage of the trigonometric interpolation is that its transfer function is close to being ideal. However, its disadvantage is that it requires too many multiplications at each time step δt , i.e. $2Q^I + 1$.

An alternative approach is the polynomial interpolation, which ensures continuity up to γ^{th} order derivatives at time $n\Delta t$. The polynomial interpolation has a stability problem. The interpolation is said to be stable if a bounded discrete process after the interpolation remains bounded as time increases to infinity. The interpolation stability is also the stability of the estimated derivatives up to the γ^{th} order. If a process $Y(n\Delta t)$ to be interpolated consists of all zero values and non-zero initial derivatives, then one can have

$$y^{(*)}(n\Delta t) = Dy^{(*)}[(n-1)\Delta t] \quad (67)$$

where $y^{(*)}(n\Delta t)$ denotes the vector of derivatives up to γ^{th} order

$$y^{(*)}(n\Delta t) = \begin{bmatrix} y(n\Delta t) \\ y(n\Delta t) \\ \vdots \\ y^{(\gamma)}(n\Delta t) \end{bmatrix} \quad (68)$$

and D is an γ, γ matrix. Therefore, the interpolator is stable if all the absolute values of the eigenvalues of the matrix D are less than 1.

The interpolation between $y(n\Delta t)$ and $y[(n+1)\Delta t]$ according to $y(n\Delta t)$, $\dot{y}(n\Delta t)$, $y[(n+1)\Delta t]$ and $y[(n+2)\Delta t]$ has the form given below

$$y[(n+\alpha)\Delta t] = c_3\alpha^3 + c_2\alpha^2 + c_1\alpha + c_0 \quad \text{for} \\ n = 0, 1, \dots, \quad \text{and} \quad 0 \leq \alpha \leq 1 \quad (69)$$

where the coefficients c_i ($i = 0, 1, 2, 3$) are obtained by a matching method. A mathematical manipulation leads to another double subscripted parametric model:

$$y[(n+\alpha)\Delta t] = \sum_{r=0}^2 I_{r\alpha} y[(n+r)\Delta t] \\ + I'_\alpha \dot{y}(n\Delta t) \quad (70)$$

where the model coefficients are given by

$$I'_\alpha = \left(\frac{1}{2}\alpha^3 - \frac{3}{2}\alpha^2 + \alpha \right) \Delta t$$

$$I_{0\alpha} = \frac{3}{4}\alpha^3 - \frac{7}{4}\alpha^2 + 1$$

$$I_{1\alpha} = -\alpha^3 + 2\alpha^2$$

and

$$I_{2\alpha} = \frac{1}{4}\alpha^3 - \frac{1}{4}\alpha^2 \quad (71)$$

and the derivative is given by a recursive model,

$$\dot{y}(n\Delta t) + d'y[(n-1)\Delta t] = \sum_{r=-1}^1 d_r y[(n+r)\Delta t] \quad (72)$$

where the coefficients are given by $d' = 1/2$, $d_{-1} = -5/(4\Delta t)$, $d_0 = 1/\Delta t$ and $d_1 = 1/(4\Delta t)$. The initial derivative of $y(0)$ can be obtained by a cubic interpolation of the points $y(0)$, $y(\Delta t)$, $y(2\Delta t)$ and $y(3\Delta t)$. Concerning the stability, $D = -0.5$ of eqn (67) satisfies the necessary stability condition.

This method offers simplicity as it is based on smooth fitting without taking into consideration the frequency contents of the time series. A problem of spectral contamination after the interpolation may be introduced. In order to reduce the error induced by interpolation, it is recommended that the time series to be interpolated must have insignificant level of energy in the high frequency range, e.g. in the frequencies higher than 0.4 of the Nyquist frequency.

8 DISCRETE DIFFERENTIATION MODELS

The numerical differentiation by the central difference method or other related methods may be viewed as another form of parametric model in which a parent process is transformed to its derivatives, e.g. from wave particle velocities to wave particle accelerations. A *two-sided discrete differentiation model* may be defined utilizing the central difference method:

$$y(n\delta t) = \sum_{r=1}^Q D_r \{ y[(n+r)\delta t] - y[(n-r)\delta t] \} \quad (73)$$

where

$$D_1 = \frac{1}{2\delta t} \quad \text{if } Q = 1,$$

or

$$\left. \begin{aligned} D_1 &= \frac{2}{3\delta t} \\ D_2 &= -\frac{1}{12\delta t} \end{aligned} \right\} \quad \text{if } Q = 2 \quad (74)$$

The choice of order Q directly affects the accuracy and the error is given by $e = O(\Delta t^{Q+1})$

Similarly, the *one-sided discrete differentiation model* is defined by a backward or a forward difference scheme,

$$\dot{y}(n\delta t) = \sum_{r=0}^Q D_r y[(n-r)\delta t] \quad (75)$$

where

$$\left. \begin{aligned} D_0 &= -\frac{1}{\delta t} \\ \text{and} \\ D_1 &= \frac{1}{\delta t} \end{aligned} \right\} \quad \text{if } Q = 1, \quad (76)$$

or

$$\left. \begin{aligned} D_0 &= -\frac{3}{2\delta t} \\ D_1 &= \frac{2}{\delta t} \\ D_2 &= -\frac{1}{2\delta t} \end{aligned} \right\} \quad \text{if } Q = 2 \quad (77)$$

The error in a one-sided differentiation model is expressed by $\epsilon = O(\Delta t^Q)$.

The discrete differentiation models expressed by eqns (73) and (75) appear to have the same form as the discrete convolution model given by eqn (24). However, there are some essential differences between these two models; namely,

- (1) The inverse Fourier transform of the coefficients in a discrete differentiation model approximates the target transfer function in the low frequency range (i.e. near to the zero frequency), whereas a discrete convolution model has a valid frequency range that spans the entire frequency up to the Nyquist frequency except at very low frequencies.
- (2) The valid maximum frequency of the discrete differentiation model is a fraction of the Nyquist frequency. Hence, it is recommended to use very small time increments to increase the Nyquist frequency and consequently to increase valid minimum frequency. Recall that the discrete convolution model requires a large time increment for a correct representation of the transfer function at low frequencies. The salient features of these models are listed in Table 1.

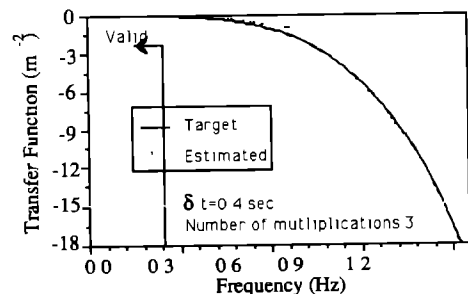


Fig. 27. Second-order feedback transfer function by discrete differentiation model.

Table 1. Discrete convolution and discrete differentiation models

Model name	Application	Time increment	Valid max frequency	Valid freq range	Model order
Discrete convolution	Wide	Large	Same as Nyquist freq.	All, except very low freq	High
Discrete differentiation	Limited	Small	Less than Nyquist freq	Low freq	Low

An example of the application of the discrete differentiation model is the second-order feedback transfer function $h_{\theta}^{[2]}(f)$ (described in the following section), which is given in terms of a fourth-order derivative. It is noted in Fig. 27 and in Fig. 28, which is a closer look at the low frequency part of Fig. 27, that the estimated transfer function by the discrete differentiation model is close to the target transfer function only in the frequency range smaller than 0.25 Hz for the model time increment δt equal to 0.4 seconds. At each time interval only three multiplications and additions are required for the simulation.

9 HYBRID MODELS

A hybrid model is proposed in which a combination of the discrete convolution and differentiation models is utilized to benefit from the individual features of these models. The formulation of a hybrid model is illustrated by the following example.

The preceding wave-related time processes were generated in this study by linear transformation of the wave surface fluctuation at a reference location. These processes are referred to as a space-fixed location. But in the case where a body experiences large excursions, it is important to evaluate the wave-related processes at the displaced position of the body, e.g. a TLP. Typically, the wave drag force and the diffraction force must be evaluated at the instantaneous displaced position of the platform.

Let $y(t)$ be a wave-related process, which may represent a time process for wave surface elevation, wave particle velocity, wave particle acceleration or diffraction force, at a space-fixed location coincident

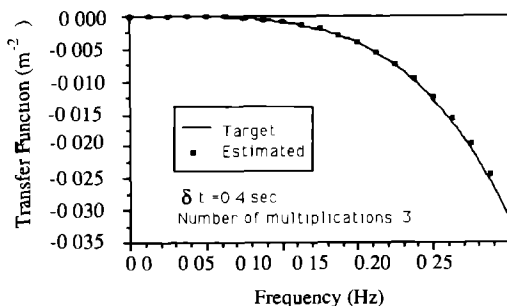


Fig. 28. Second-order feedback transfer function by discrete differentiation model

with the initial location of the center of a structural component. And let $y(t, \xi)$ be the same wave-related process evaluated at ξ which is the instantaneous displacement of the structural component from its initial location along the wave propagation direction. $y(t)$ is linearly related to the wave surface fluctuation at a reference location, $\eta(t)$, expressed as

$$y(t) = L(\eta(t)) \quad (78)$$

Then $y(t, \xi)$ must be

$$y(t, \xi) = L(\eta(t, \xi)) \quad (79)$$

where $\eta(t, \xi)$ is the wave surface elevation at a location ξ apart from the reference location along the direction of wave propagation.

A mathematical manipulation leads to

$$y(t, \xi) = y(t) + \theta(t)\xi(t) + \theta^{[2]}(t)\xi^2(t) + \quad (80)$$

y as a function of structural displacement in terms of y evaluated at the initial structural plus feedback terms.²⁹ The feedback coefficients, however, are time-dependent, and are linear transforms of the process at the structural initial location. The time processes representing the feedback coefficients can be simulated by discrete convolution models. In the deepwater case, these coefficients can be written as

$$\theta(t) = \int_0^{\infty} h_{\theta}(\tau) \left[\frac{dy}{dt}(t - \tau) + \frac{dy}{dt}(t + \tau) \right] d\tau \quad (81)$$

with

$$h_{\theta}(t) = 2 \int_0^{+\infty} 2\pi f \cos(2\pi f t) df \quad (82)$$

and

$$\theta^{[2]}(t) = -\frac{1}{g^2} \frac{\partial^4 y(t)}{\partial t^4} \quad (83)$$

The time series of the second-order feedback coefficients can be realized by a discrete differentiation model.

The first-order feedback coefficient may be regarded as the convolution (the corresponding transfer function is $2\pi f$) of the time derivative of the input load. The discrete convolution with the transfer function as $2\pi n \Delta f$ has been shown in eqn (53). Hence, a combination of eqn (53) for the discrete convolution and eqn (73) for the

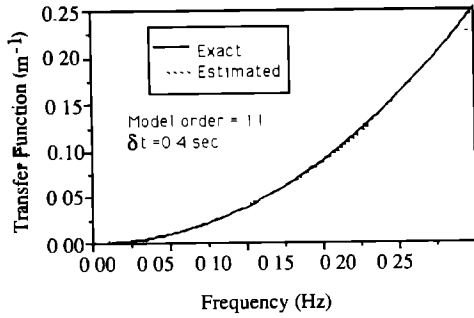


Fig. 29. First-order feedback transfer function by hybrid model

discrete differentiation provides

$$\theta(n\delta't) = h_0 y(n\delta't) + \sum_{r=1}^{Q/2} h_{2r} \{ y[(n+2r)\delta't] + y[(n-2r)\delta't] \} \quad (84)$$

where order Q is an even number, and the model coefficients are given by

$$h_0 = \frac{\pi}{4g\delta't^2} \quad (82)$$

$$h_{2r} = \frac{1}{\pi g\delta't^2} \left[\frac{1}{(2r+1)^2} - \frac{1}{(2r-1)^2} \right] \quad \text{and} \quad (86)$$

$$h_Q = \frac{-1}{\pi g\delta't^2(Q-1)^2} \quad (87)$$

Both the valid maximum and minimum frequencies (f_{max} and f_{min}) should be taken into consideration when making a choice concerning the time increment and the order of a hybrid model. A recommended value of the time increment is given here:

$$\delta't = \frac{1}{10f_{max}} \quad (88)$$

The order Q of the hybrid model largely depends on the minimum frequency f_{min} . An empirical relationship describing the order Q in terms of $\delta't$ and f_{min} established during the course of this study is

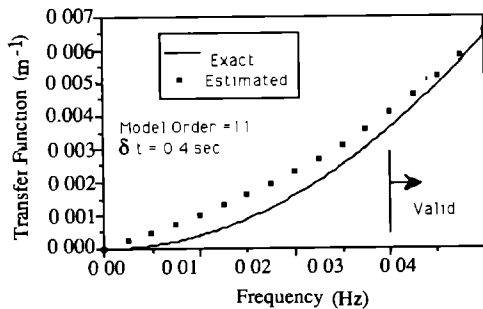


Fig. 30. First-order feedback transfer function by hybrid model

given below:

$$Q = \frac{1}{8\delta'tf_{min}} \quad (89)$$

For example, if the time increment of a hybrid model is 0.4 seconds and the model order is 10, the valid frequency range is 0.03 Hz to 0.25 Hz (Figs 29 and 30).

10 EXAMPLE

The dynamic response of a tension leg platform under a random wave field in the time domain is an example used herein to illustrate the application of the parametric models to offshore engineering. The example of a TLP has been selected as all the models discussed in this paper are needed for the simulation of a TLP response in the time domain. The simulation of wind and wave-drift forces, which are important to the TLP motions, is beyond the scope of this presentation. A typical TLP configuration and the front view of the four-column TLP are shown in Figs 31a and 31b. The TLP is modelled as a six-degree-of-freedom rigid body.

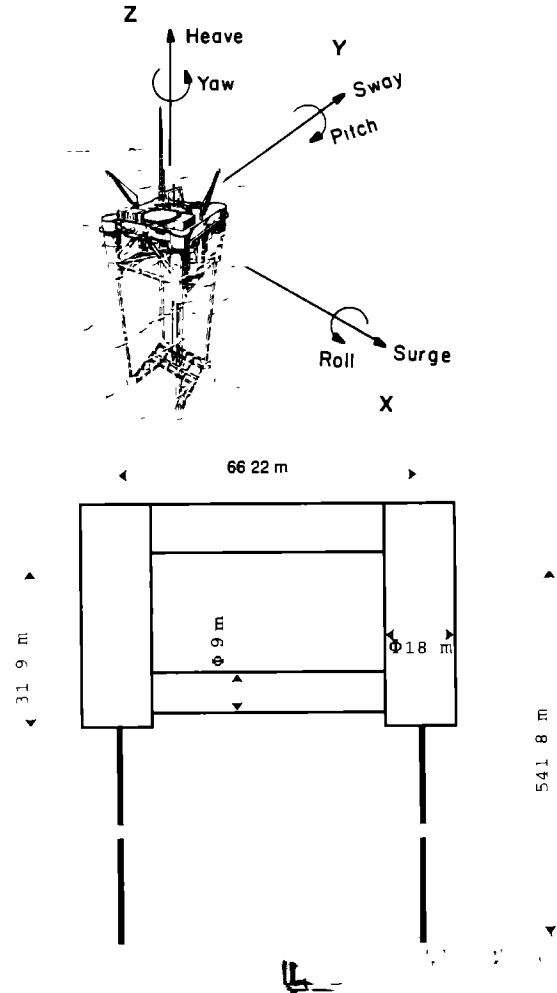


Fig. 31. a Schematic diagram and degrees of freedom of a TLP b Example of a TLP elevation

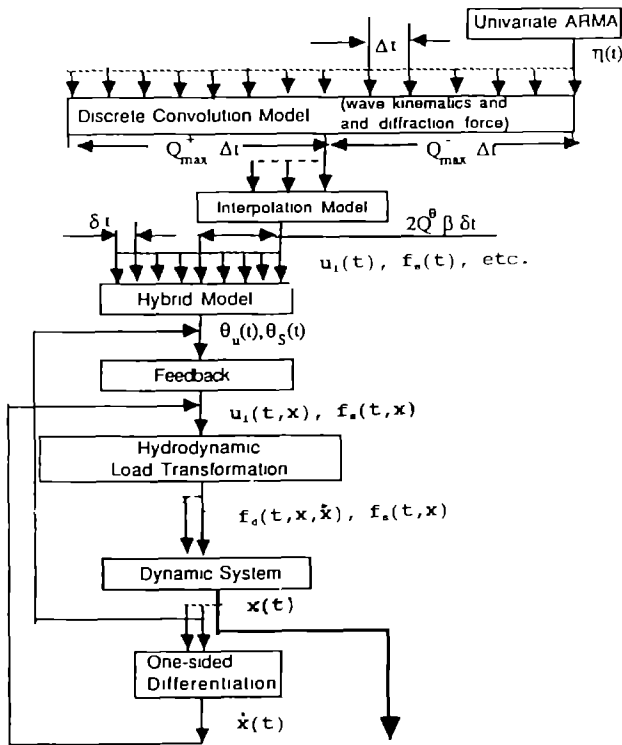


Fig. 32. Synthesis of parametric models for TLP response evaluation

The basic equations of motion are expressed in the following matrix form

$$Mx(t) + C_{str}x(t) - f_R(x, \dot{x}) + K(x)x(t) = f_s(t, \dot{x}) + f_d(t, x, \dot{x}) \quad (90)$$

In the left-hand side of the preceding equation, $x(t)$ is the rigid body displacement, M , C_{str} and $K(x)$ are the mass, structural damping and nonlinear stiffness matrices (all 6×6), and $f_R(x, \dot{x})$ is the radiation force due the platform oscillation. In the right-hand side, $f_s(t, \dot{x})$ and $f_d(t, x, \dot{x})$ are the wave diffraction and drag forces computed at the displaced position of the platform, x . The global diffraction force can be directly formulated from global diffraction transfer functions. The drag force is computed by discretizing the entire platform in a number of elements. The global drag

force is the summation of the drag forces on each element

The process of simulating these forces and associated responses is illustrated by Fig 32, in which the vertical direction represents the flow of the computational procedure, and the horizontal direction indicates the time shift among various parametric models. The explanation of each block of this figure is given below:

- 'Univariate ARMA' The time series of the wave surface fluctuation at a reference location is generated by an ARMA model designed to represent a prescribed design wave spectrum. The horizontal reference location is generally the centre of the TLP. The time step is Δt , which is determined by the maximum frequency of interest as $1/3$ of $1/(2\Delta t)$. A segment of wave surface fluctuation based on JONSWAP wave spectrum is plotted in Fig. 33.
- 'Discrete Convolution Model' The discrete convolution model, is used to simulate the time series of the global diffraction force $f_s(t)$ and the wave particle velocity at the i th element center $u_i(t)$ and wave surface elevation at the i th column $\eta_i(t)$ based on the wave surface fluctuation at the reference location. A segment of diffraction force time history is shown in Fig. 34. The time increment remains Δt . These processes are related to the initial location of the structure. Altogether, many time series should be simulated using individual discrete convolution models. Each model has its own best orders Q^+ and Q^- . In the computer code, it is recommended to use flexible length vectors to store these model coefficients for saving CPU time and storage. The maximum time window in the discrete convolution models is $(Q_{max}^+ + Q_{min}^-)\Delta t$.
- 'Interpolation Model' The time increment of the above time processes is changed to a small value δt , which must satisfy the requirement in the solution of dynamic eqn (90).
- 'Hybrid Model' This model facilitates computation of the time-dependent feedback

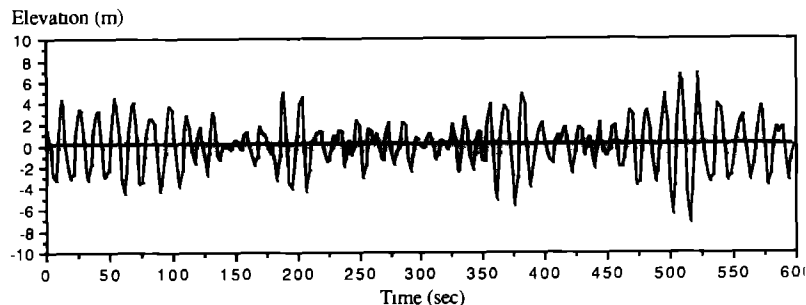


Fig. 33. Time history of wave surface elevation

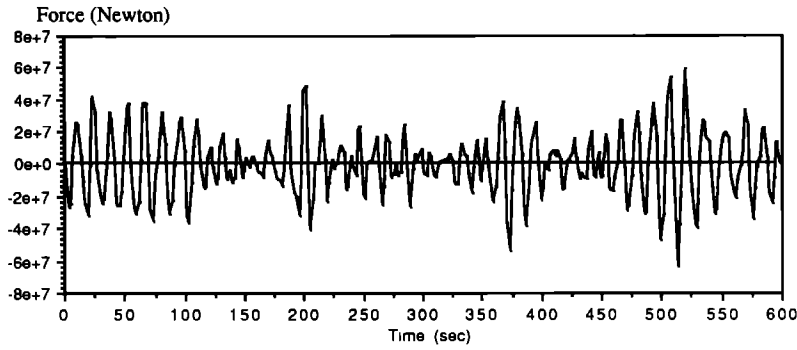


Fig. 34. Time history of surge diffraction force.

coefficients, $\theta_{ui}(t)$ and $\theta_s(t)$, as linear transforms of the wave particle velocities or wave forces. The hybrid models involve fewer multiplications. The small time increment required by the hybrid model is satisfied since it is introduced after interpolation.

- (e) 'Feedback': From the wave processes related to the structural initial position, the displacements of the platform at the previous time step or previous iteration and the feedback coefficients, we can obtain the corresponding processes $f_s(t, x)$ and $u_i(t, x)$ at the displaced position of the platform.
- (f) 'Hydrodynamic Load Transformation': The drag force is quadratic in terms of the relative fluid-structure velocity

$$f_d(t, x, \dot{x}) = \sum T_i C_{D_i} [u_i(t, x) - T_i^T \dot{x}(t)] \times |u_i(t, x) - T_i^T \dot{x}(t)| \quad (91)$$

in which T_i and T_i^T denote the local to global and global to local coordinate transformation matrices, respectively, C_{D_i} is the component drag coefficient.

- (g) 'Dynamic System': In the discrete form, by introducing the retardation model, the dynamic equations of motion can be recast into

$$(M + \dot{A})x(m\delta t) + (C_{str} + C_0)\dot{x}(m\delta t) + K(x)x(m\delta t) = f_s(m\delta t, x) + f_d(m\delta t, x, \dot{x}) - \sum_{r=1}^Q C_r x[(n-r)\delta t] \quad (92)$$

in which the symbols for the retardation have been defined previously. Considering the stiffness $K(x)$, as well as the wave diffraction and drag force being displacement-dependent, an iterative scheme is needed for response evaluation. Li and Kareem²⁸ suggested a special Newmark β form, in which the response in the present time becomes a linear combination of the response and the loads in the past time history. Since the past loads only depend on the past response, no iteration is

needed. This approach is based on the central difference method, which was cast as a two-sided difference model in eqn (74). A time shift leads to the following

$$x[(m-1)\delta t] = \frac{x(m\delta t) - x[(m-2)\delta t]}{2\delta t}$$

and

$$\ddot{x}[(m-1)\delta t] = \frac{x(m\delta t) - 2x[(m-1)\delta t] + x[(m-2)\delta t]}{\delta t^2} \quad (93)$$

Let the left-hand side of eqn (92) be $f(m\delta t, x)$. We can recast the dynamic equation into

$$\begin{aligned} & \left(\frac{M + \dot{A}}{\delta t^2} + \frac{C_{str} + C_0}{2\delta t} \right) x(m\delta t) \\ & = f[(m-1)\delta t, x] + \frac{2M}{\delta t^2} x[(m-1)\delta t] \\ & + \left(\frac{M + \dot{A}}{\delta t^2} + \frac{C_{str} + C_0}{2\delta t} \right) x[(m-2)\delta t] \end{aligned} \quad (94)$$

Hence, the solution of the final equations of motion is a combination of the discrete retardation and differentiation models.

- (h) 'One-sided Differentiation': The displacement response has to be further transformed to velocity response for formulation of the drag force in the next time step. Since the displacement in the future is unknown, one-side differentiation is used. Hence, in the same algorithm, we have two kinds of parametric models used to describe the response velocities from the displacements: two-sided differentiation model in 'Dynamic System' and one-sided differential model for drag force simulation. The preceding discussion illustrates how the various parametric models serve as means of simulating time series representing wave height, wave kinematics and wave loads and how these models can be integrated in the overall computation of the platform response.

11 CONCLUDING REMARKS

Various parametric models are presented that offer computationally efficient means of generating time histories of wave surface profile and related wave kinematics and load effects. The models are placed in three categories, namely ARMA, convolution and interpolation schemes. In the following a summary of these models is presented that highlights the key features of the models, their order and associated errors.

(1) Recursive Simulation of Uni-variate Time Series. Uni-variant ARMA models are utilized for simulating the wave surface elevation consistent with a prescribed spectral description. It is desirable to design AR and MA models with the lowest orders and minimum model error. This requirement may be satisfied if the maximum entropy method is utilized. However, the algorithm for the general MEM method involves a significant level of computational effort. In this study a two-stage model fitting approach is used in which the maximum entropy is satisfied with some imposed restrictions. Thus, the decision concerning the ARMA order becomes a selection by the user from a host of multiple options. This is accomplished through a direct comparison of the target and estimated spectra, or other criteria, e.g. goodness of fit may be utilized.

(2) Non-recursive Simulation by Linear Transformations. The second application involves simulation of linearly related processes. The common form of a linear transformation may be the convolution, based on which the discrete convolution model has been defined. This non-recursive model has two forms, namely the model representing a convolution of an infinite and finite duration waveform and the model representing a convolution of two infinite duration waveforms. The application of the former seems to be limited since the estimated transfer function slowly converges or even estimates fail to converge to the target transfer function. The latter is widely used in this study, mainly for simulating wave kinematics and diffraction forces based on the wave surface elevation at a reference location. Since this non-recursive model is only a discrete and truncated version of the convolution integral over an infinite time period, the model order may be determined by the decay of the convolution kernel. This model may be viewed as a filtered output of the past, the present and the future time histories of a parent process.

In the case of radiation force simulation, the future time history of the response of the parent process is unknown. Thus the retardation model is introduced in a manner such that the radiation force is a linear combination of the past and the present time histories of the response. The associated filter is developed by sacrificing slightly the accuracy of the frequency-dependent added mass. However, the accuracy of the added mass may not be very important. A better description of the radiation damping as a function of

frequency is more important because at the low natural frequency of a compliant structure it is nearly zero and at wave frequencies it could lead to higher values.

Discrete differentiation is another non-recursive model used here in the context of linear transformation. It has the same form as the discrete convolution model, however, its transfer function is only valid in the low frequency range. This model is used in this study for several cases, e.g. to simulate the velocity response from the displacement response. The time integration scheme for the solution of the dynamic equations of motion can be based on this model.

A hybrid model is introduced which combines the attractive features of the discrete convolution and differentiation models. The time variant first-order feedback coefficients, needed to describe the wave loading at the instantaneous displaced position of the platform, are efficiently evaluated by means of a hybrid model.

(3) Parametric Interpolation Model: Interpolation of the time histories is carried out by parametric models. The transfer function of an interpolation model is the same as that of a lowpass filter. Both trigonometric and polynomial interpolation techniques are utilized in this study.

The parametric models presented in this paper offer a very efficient computational tool for the time domain analysis of wave load effects on offshore platforms.

ACKNOWLEDGEMENTS

Financial assistance for this research was provided by the National Science Foundation Grant BCS-9096274 (BCS-835222), and matching funds from several major oil companies. Any opinions, findings, and conclusions or recommendations expressed in this paper are the writers' and do not necessarily reflect the views of the sponsors.

REFERENCES

- 1 Shinozuka, M., Simulation of Multivariate and Multi-dimensional Random Processes. *J. Acoustic Society of America*, **49**(1) Part 2 (1970) 357-67.
- 2 Shinozuka, M. & Jan, C-M., Digital Simulation of Random Processes and its Applications. *J. Sound and Vibration*, **25**(1) (1972) 111-28.
- 3 Wittig, L.E. & Sinha, A.K., Simulation of Multi-correlated Processes Using the FFT Algorithm. *J. Acoustical Society of America*, **58** (1975) 630-3.
- 4 Kareem, A. & Dalton, C., Dynamic Effects of Wind on Tension Leg Platforms. *Proceedings of Ocean Structural Dynamics Symposium '82*, Oregon State University, Corvallis, Oregon, 1982.
- 5 Borgman, L.E., Ocean Wave Simulation for Engineering Design. *J. Waterway and Harbors Div., ASCE*, **65** (1969) 557-83.

6. Reed, D.A. & Scanlan, R.H., Autoregressive Representation of Longitudinal, Lateral, and Vertical Turbulence Spectrum *J Wind Engineering Industrial Aerodynamics*, **17** (1984) 199–214
7. Smaras, E., Shinozuka, M. & Tsurui, A., ARMA Representation of Random Processes *J Engineering Mechanics, ASCE*, **111** (1985) 449–61.
8. Spanos, P.D. & Mignolet, M., Z-Transform Modelling of P–M Wave Spectrum. *J. Engineering Mechanics, ASCE*, **112** (1986) 745–59
9. Naganuma, T., Deodatis, D. & Shinozuka, M., ARMA Model for Two-Dimensional Processes *J Engineering Mechanics, ASCE*, **113** (1987) 234–51
10. Kareem, A. & Li, Yousun, Stochastic Response of a Tension Leg Platform to Wind and Wave Loads *Department of Civil Engineering Technical Report No UHCE 88-18*, University of Houston, TX, 1988
11. Samii, K. & Vandiver, J.K., A Numerically Efficient Technique for the Simulation of Random Wave Forces on Offshore Structures *OTC Paper 4811, Proceedings of the Offshore Technology Conference*, Houston, TX, 1984
12. Spanos, P.D., ARMA Algorithms for Ocean Wave Modelling, *J Energy Resources Technology, ASME*, **10** (1983) 530–3
13. Wheeler, J.D., Method for Calculating Forces Produced by Irregular Waves. *J Petroleum Technology*, 1970, 360–3.
14. Burke, B.G. & Tighe, J.T., A Time Series Model of Dynamic Behavior of Offshore Structures, *Society of Petroleum Engineering J*, February 1972, 168–70.
15. Houmb, O.G. & Overvik, T., Some Application of Maximum Entropy Spectral Estimation to Ocean Waves and Linear Systems Response in Waves, *Applied Ocean Research*, **3** (1981) 154–62
16. Van den Boss, A., Alternative Interpretation of Maximum Entropy Spectral Analysis *IEEE Transactions on Information, Theory*, **II-7** 493–4.
17. IMSL, *Library Reference Manual*. IMSL, Inc, Houston, TX, 1980
18. Cadzow, J.A., High Performance Spectral Estimation – A New ARMA Method *IEEE Trans. on Acoust., Speech, Sig. Proc. ASSP-28*, 1980 pp. 524–9.
19. Spanos, P.D. & Schultz, K.P., Two-Stage Order-of-Magnitude Matching for the Von Karman Turbulence Spectrum. *Proceedings of the 4th International Conference on Structural Safety and Reliability*, Kobe, Japan, 1985, pp 211–17.
20. Chakrabarti, S.K., *Hydrodynamics of Offshore Structures*, Springer-Verlag, New York, 1987
21. Ronzanov, I.U.A., *Stationary Random Processes*. Holden-Day, San Francisco, CA, 1967
22. Li, Yousun & Kareem, A., ARMA Modelling of Random Wind and Wave Fields, *Engineering Mechanics – Sixth Conference, Abstracts*, ASCE, Buffalo, NY, New York, 1987
23. Li, Yousun & Kareem, A., ARMA Systems in Wind Engineering, *Probabilistic Engineering Mechanics*, **5**(2) (1990) 50–9.
24. Roger, M., Fatigue Analysis for Deepwater Fixed Bottom Platform, *OTC Paper 2051*, Offshore Technology Conference, Houston, TX, 1974
25. Brigham, E.O., *The Fast Fourier Transform*, Prentice-Hall, Inc, 1974.
26. Papoulis, A., In *Probability, Random Variables and Stochastic Processes* McGraw-Hill Book Company, 1965
27. Ogilvie, T.F., Recent Progress Towards the Understanding and Prediction of Ship Motions, *Fifth Symposium on Naval Hydrodynamics*, Bergen, Norway, 1964
28. Li, Yousun & Kareem, A., Recursive Modeling of Dynamic Systems, *J. Engineering Mechanics, ASCE*, **116** (1989) 660–79
29. Li, Yousun & Kareem, A., Computation of Wave-induced Drift Forces Introduced by Displaced Position of Compliant Offshore Platforms, *J Offshore Mechanics Arctic Engineering*, **114** (1992) 175–84.